Supplementary Information

Table S1. Content and conjugation efficiency of metformin and ICG in PLGA nanoparticles.

Encapsulation efficiency was calculated using the formula mentioned in Materials and Methods.

	Total Amount (mg)	Encapsulated Amount (mg)	Encapsulation Efficiency (%)
Metformin	2.00	0.852	42.6
ICG	2.00	0.820	41.0
PLGA	5.00	3.810	76.2

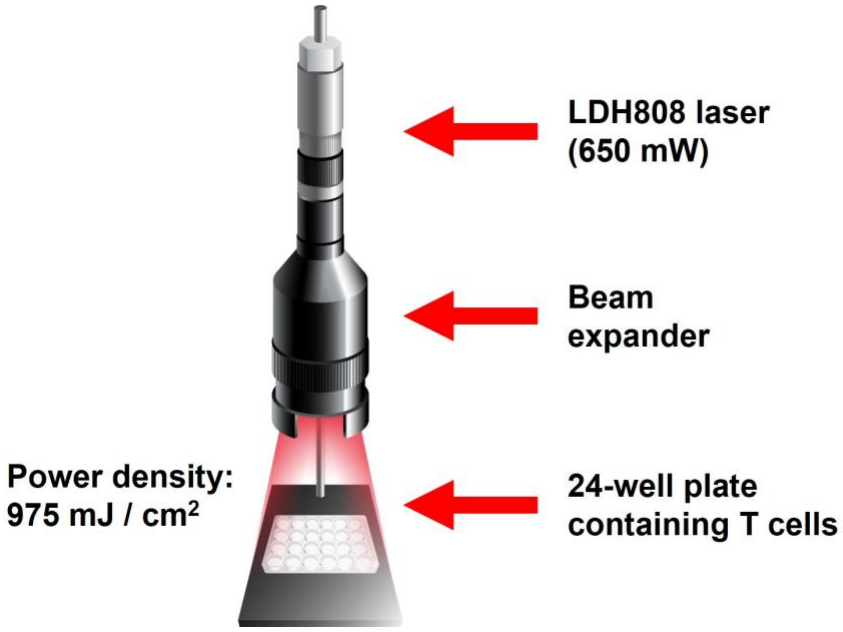

Figure S1. Setup of NIR laser treatment. The LDH808 laser was attached to a metal rod for sturdiness. The beam expander was calibrated to precisely encompass the area of one test group at a time with the laser's trajectory. The distance between the 24-well plate and the end of the beam expander was 25 cm.

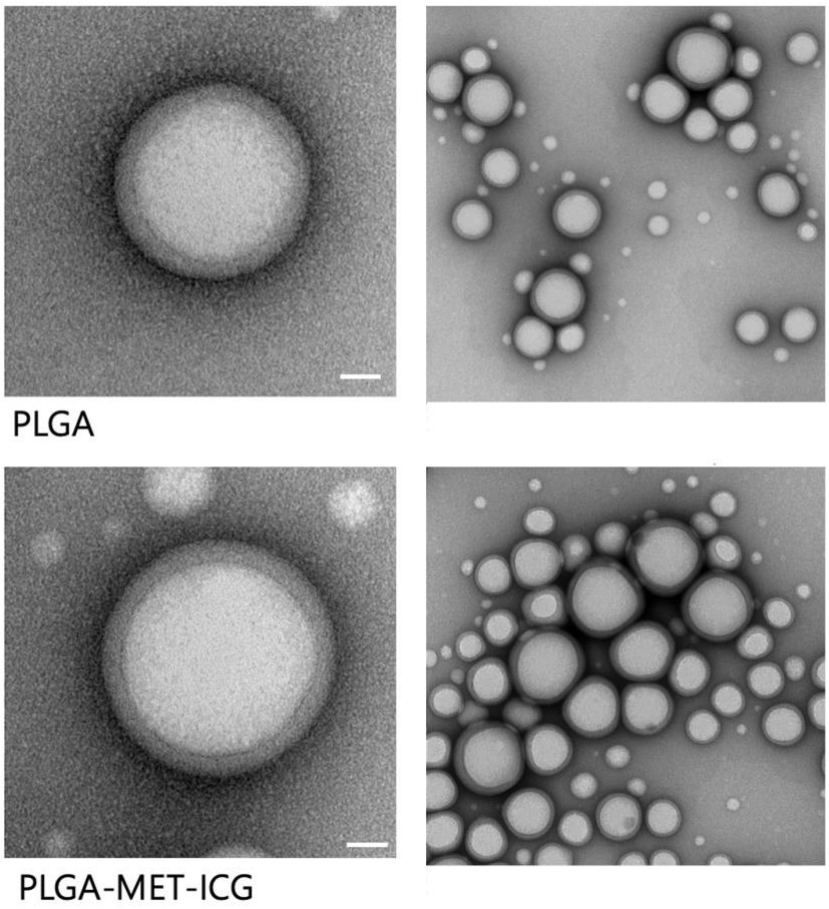

Figure S2. Additional TEM images of PLGA with and without metformin and ICG encapsulation. The visible change in morphology suggests the successful encapsulation of metformin and ICG. Scale bar = 20 nm for the left two images that show a single nanoparticle. Scale bar = 100 nm for the right two images that show multiple nanoparticles.

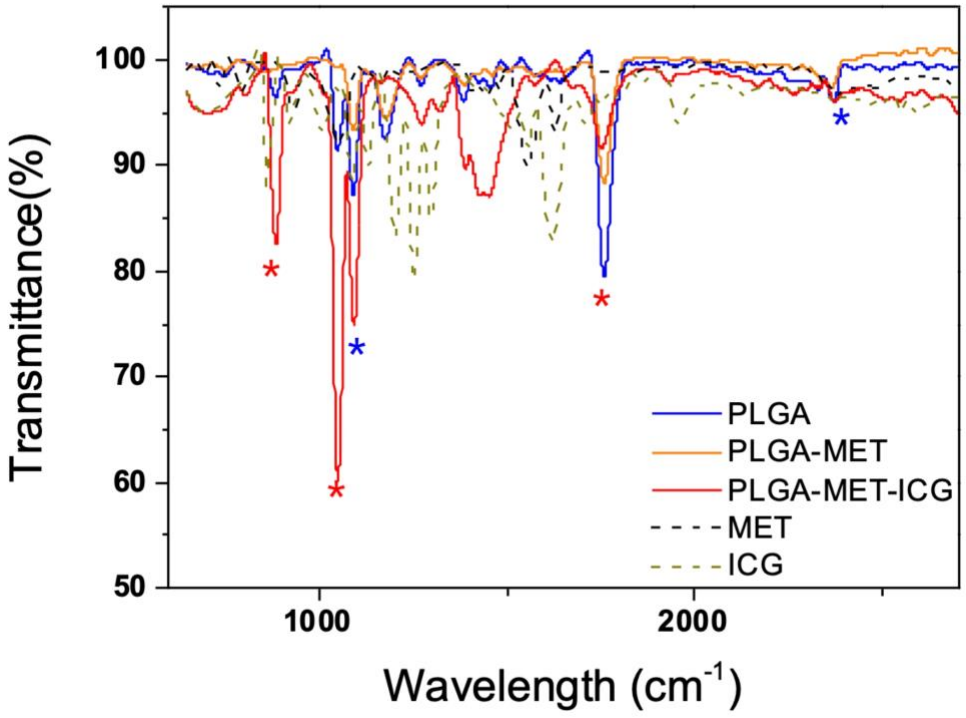

Figure S3. Fourier Transform Infrared Spectroscopy (FTIR) analysis of free metformin, free ICG, PLGA-MET, and PLGA-MET-ICG. The characteristic absorbance peaks of free metformin and ICG are consistent among PLGA-metformin and PLGA-metformin-ICG.

Table S2. Mouse primer sequences used for real-time PCR. Primers were sequenced based on information obtained from UniProt and synthesized by BIONICS (Seoul, Korea).

Target gene	Sequence (5'→3')
GAPDH	Forward: TGCTGAGTATGTCGTGGAGT Reverse: AGATGATGACCCTTTTGGCTC
IL-1β	Forward: GCATGGTATGGACTGTGGAC Reverse: GCAATATCCTCTGGGTCCTG
TNF-α	Forward: TGTCTACTGAACTTCGGGGT Reverse: GAGGGTCTGGGCCATAGAA
IL-6	Forward: CTTCACAAGTCGGAGGCTTAAT Reverse: AGTCGATCATCGTTGTTCATAC
Arg-1	Forward: GCAGAGGTCCAGAAGAATGG Reverse: ACACATAGGTCAGGGTGGAC
IL-4	Forward: AGATGGATGTGCCAAACGTC Reverse: AATATGCGAAGCACCTTGGA
IL-10	Forward: GTCATCGATTTCTCCCCTGTG Reverse: GTAGACACCTTGGTCTTGGAG
IL-22 receptor	Forward: TACGTGTGCCGAGTGAAGAC Reverse: GCCCAGATAACAGAGCAAGC
CD-23	Forward: CACAGCCTCCGATTCTCTAG Reverse: TGGAGCCCTTGCCAAAATAG

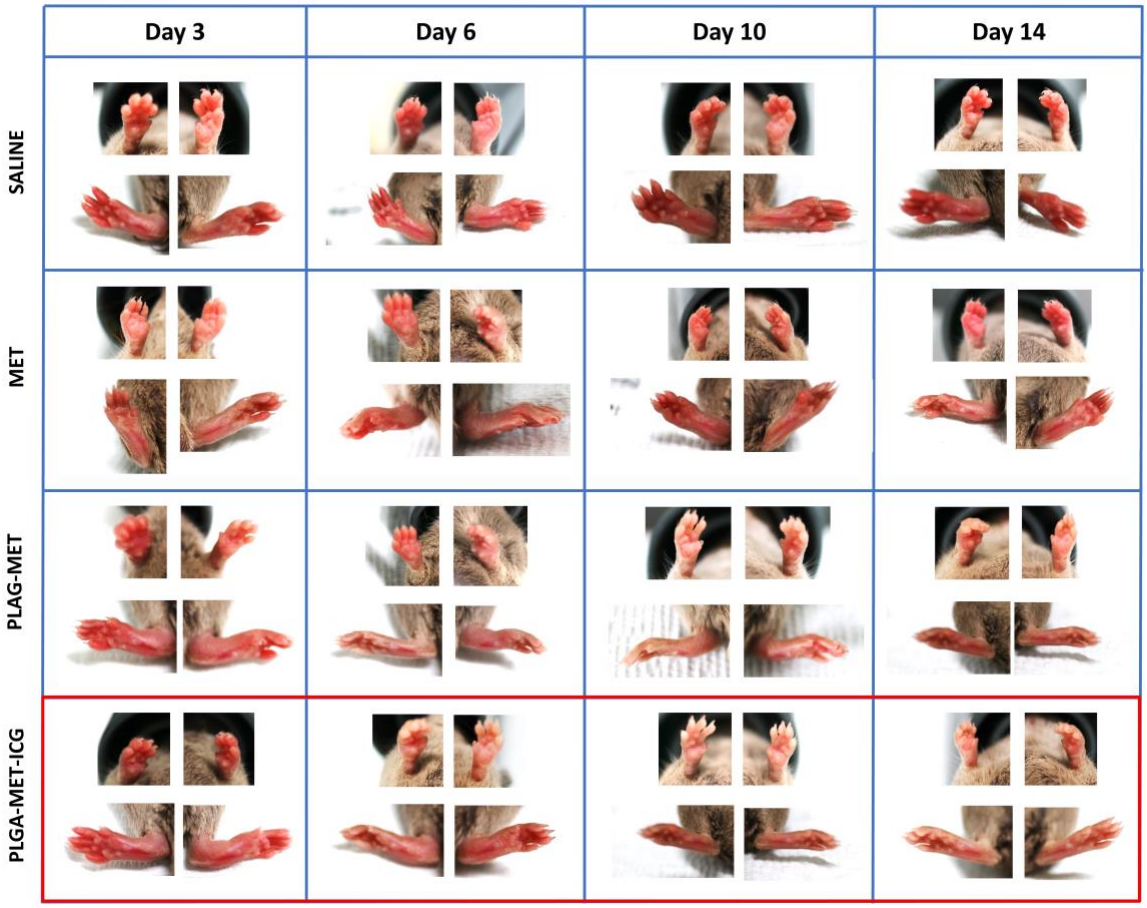

Figure S4. Paw images of CIA model mice were captured on days 3, 6, 10, and 14 days after the first injection. Images revealed a significant reduction of joint swelling in the PLGA-MET and PLGA-MET-ICG treated groups.

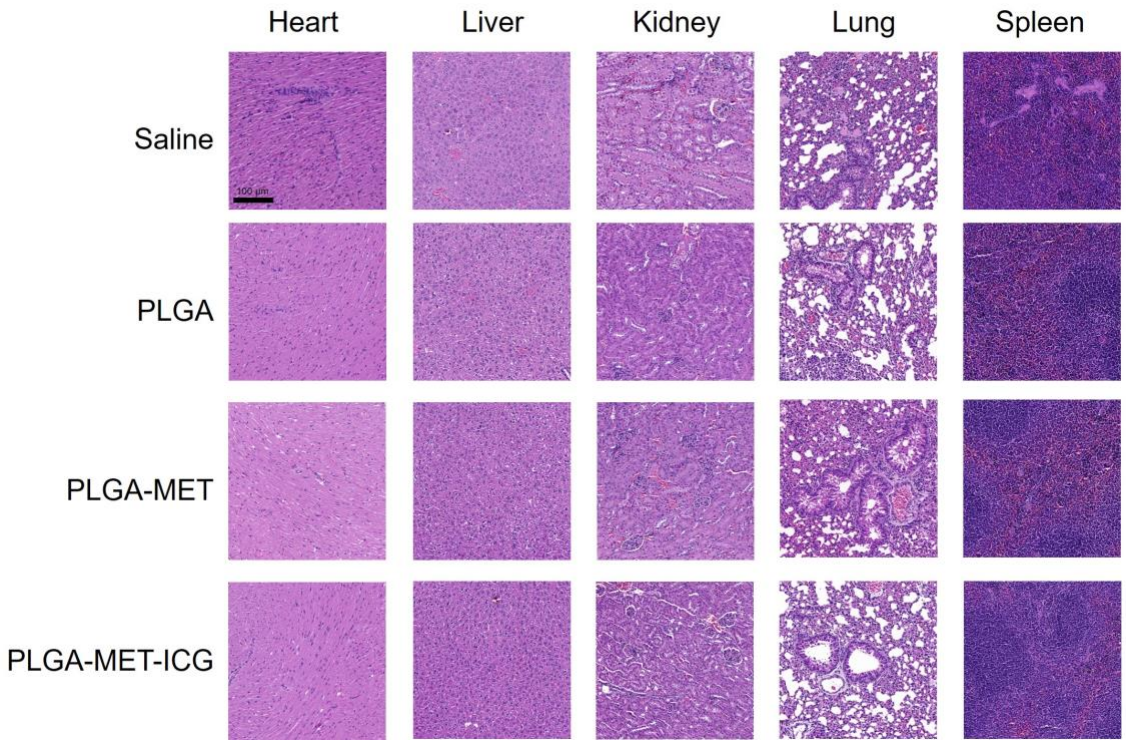

Figure S5. Representative hematoxylin & eosin (H&E) staining images of major organs (heart, spleen, liver, lungs, and spleen). Organ samples were obtained from CIA mice models at the end of the experiment.

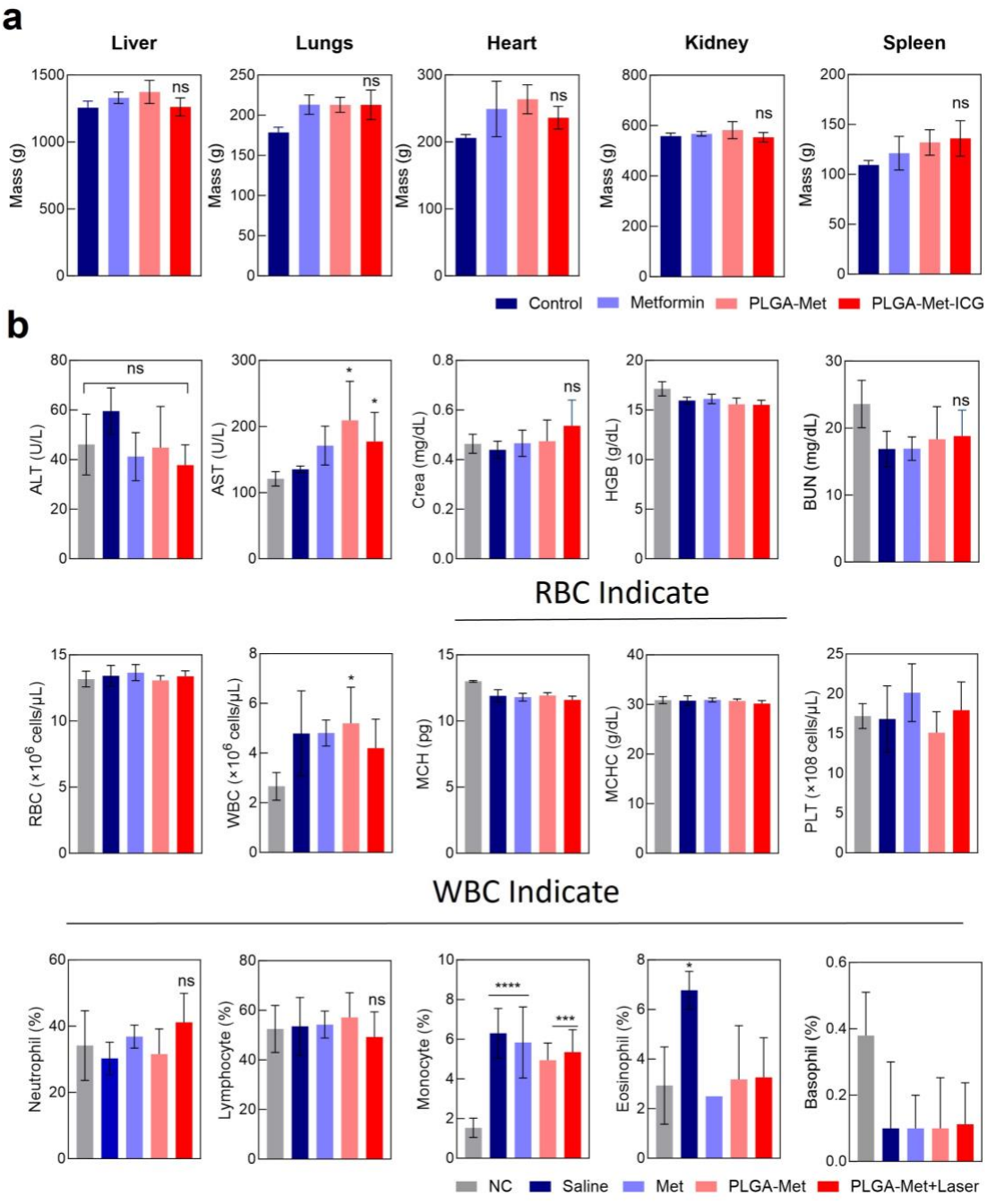

Figure S6. *In vivo* safety analysis of the nanodrug. (a) Average mass of spleen, heart, liver, lungs, and kidney of CIA mice. (b) The average levels of alanine aminotransferase (ALT), aspartate aminotransferase (AST), blood urea nitrogen (BUN), creatine, hemoglobin, red blood cells, platelet, and white blood cells. The data are presented as mean ± SEM (n = 4). *$p < 0.05$, **$p < 0.01$, and ***$p < 0.001$.

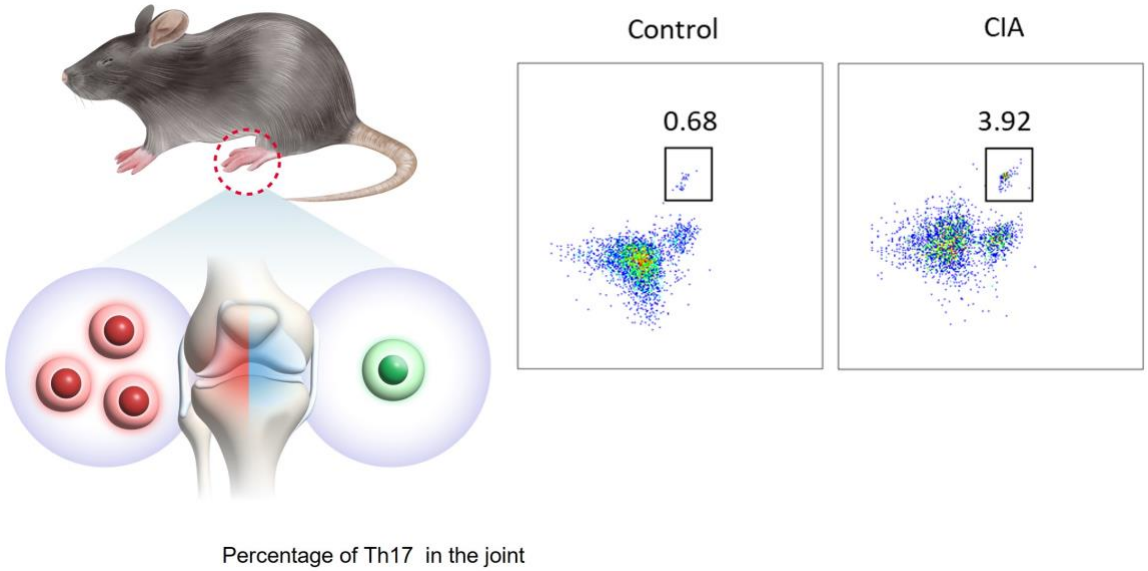

Figure S7. Detection of Th-17 levels in the inflamed synovium of mice models. Joint samples of CIA mice models were isolated to measure the changes in the Th-17 population. FACS results confirmed a notable increase in the Th-17 population in joints of mice with induced arthritis